

the ratio of tangential to normal stiffness,  $k^t/k^n$ , determines the response (Fig. 3a), which becomes nearly universal for large  $k^t/k^n$ . A spring network model (Fig. 3b) with  $\mu = \infty$  (similar to the models studied in refs 21–25) can be used to estimate the elastic moduli in the teardrop domain. Using a criterion proposed in ref. 20, a crossover from a single peak to two peaks is predicted at  $k^t/k^n \approx 0.3$ , in agreement with our numerical findings (Fig. 3a). We note that, in practice, the expected value of  $k^t/k^n$  for realistic granular matter should satisfy  $2/3 < k^t/k^n < 1$  (this follows from the Cattaneo–Mindlin model<sup>26</sup> for the contact of elastic spheres), which is well above the threshold for obtaining one peak. Here, unless otherwise noted, we use  $k^t/k^n = 0.8$ . The reduced anisotropy (for sufficiently large  $k^t/k^n$ ) is due to the horizontal projections of the static frictional forces, which compensate for the lack of normal contact forces, and can prevent the opening of horizontal contacts<sup>27</sup>, as indicated by the extended linear range in the presence of friction (Fig. 1d). In other words, static friction acts to retain an ‘effective connectivity’ between the grains when the horizontal contacts are open (as inside the teardrop), and render the system more isotropic than one would have anticipated in the absence of friction (but not exactly isotropic). Hence, for sufficiently large  $\mu$  (and realistic  $k^t/k^n$ ), the response is single-peaked. On the other hand, when  $\mu$  is small (or  $F_{\text{ext}}$  large), sliding occurs, which increases the anisotropy and leads to a crossover to a two-peaked response. This crossover is shown as a function of  $F_{\text{ext}}$  (for  $\mu = 0.2$ ) in Fig. 1b, and as a function of  $\mu$  (for  $F_{\text{ext}} = 15\text{mg}$ ) in Fig. 3c.

Polydisperse systems (with a uniform distribution of radii in the interval  $[R - \delta R, R]$ ), where  $\delta$  is a measure of the polydispersity, and  $R$  denotes the maximal particle radius, exhibit qualitatively similar behaviour to that described above. The main difference is that the range of values of  $F_{\text{ext}}$  for which the response is linear in  $F_{\text{ext}}$ , as well as the range of  $F_{\text{ext}}$  for which a single peak is obtained, decreases with increasing polydispersity, see Fig. 4a. Because the disorder in these systems induces fluctuations (which are not present in ordered systems), the results presented in Fig. 4a were smoothed by a convolution with a gaussian in the horizontal ( $x$ ) direction:  $\frac{1}{\sqrt{\pi}w} e^{-(x/w)^2}$  with  $w = 6R$ , and averaged over several realizations of the disorder (typically five).

Our results on the effect of  $F_{\text{ext}}$ ,  $\mu$  and the degree of polydispersity on the crossover are summarized in a schematic phase diagram, Fig. 4b. The diagram enables us to interpret several recent experimental studies of the response of granular materials to a localized force<sup>8–12,16,18</sup>; different experiments correspond to different regions in this diagram. A single-peaked response was observed in experiments on disordered three-dimensional (3D) packings<sup>15,17</sup> with small applied forces (a few times the particle weight), whereas multiple peaks were observed in experiments on ordered 3D packings<sup>10</sup>, where forces of a few thousand times the particle weight were applied. These peaks faded away for deeper systems. Experiments in 2D systems using photoelastic particles typically use a rather large applied force ( $F_{\text{ext}} \approx 150\text{mg}$  in refs 8, 9), required to obtain a significant photoelastic effect. The interparticle forces in the nominally ordered case are reproduced qualitatively even with frictionless particles<sup>17</sup>; however, the introduction of friction improves this agreement to an essentially quantitative level. □

Received 8 August 2004; accepted 21 February 2005; doi:10.1038/nature03497.

1. Nedderman, R. M. *Statics and Kinematics of Granular Materials* (Cambridge Univ. Press, Cambridge, 1992).
2. Savage, S. B. in *Physics of Dry Granular Media* (eds Herrmann, H. J., Hovi, J. P. & Luding, S.) 25–95 (NATO ASI Series, Kluwer, Dordrecht, 1998).
3. Jackson, R. in *Theory of Dispersed Multiphase Flow* (ed. Meyer, R. E.) 291–337 (Academic, New York, 1983).
4. Wittmer, J. P., Claudin, P., Cates, M. E. & Bouchaud, J.-P. An explanation for the central stress minimum in sand piles. *Nature* **382**, 336–338 (1996).
5. Bouchaud, J.-P., Claudin, P., Levine, D. & Otto, M. Force chain splitting in granular materials: a mechanism for large-scale pseudo-elastic behaviour. *Eur. Phys. J. E* **4**, 451–457 (2001).
6. Tkachenko, A. V. & Witten, T. A. Stress propagation through frictionless granular material. *Phys. Rev. E* **60**, 687–696 (1999).

7. Drescher, A. & de Josselin de Jong, G. Photoelastic verification of a mechanical model for the flow of a granular material. *J. Mech. Phys. Solids* **20**, 337–351 (1972).
8. Geng, J. et al. Footprints in sand: the response of a granular material to local perturbations. *Phys. Rev. Lett.* **87**, 035506 (2001).
9. Geng, J., Reydellet, G., Clément, E. & Behringer, R. P. Green’s function measurements of force transmission in 2D granular materials. *Physica D* **182**, 274–303 (2003).
10. Mueggenburg, N. W., Jaeger, H. M. & Nagel, S. R. Stress transmission through three-dimensional ordered granular arrays. *Phys. Rev. E* **66**, 031304 (2002).
11. Moukarzel, C. F., Pacheco-Martinez, H., Ruiz-Suarez, J. C. & Vidales, A. M. Static response in disk packings. *Granular Matter* **6**, 61–66 (2004).
12. da Silva, M. & Rajchenbach, J. Stress transmission through a model system of cohesionless elastic grains. *Nature* **406**, 708–710 (2000).
13. Smid, J. & Novosod, J. Pressure distribution under heaped bulk solids. In *Proc. 1981 Powtech Conf., Institution of Chemical Engineers Symp.* **63**, D3/V/1–12 (1981).
14. Brockbank, R., Huntley, J. M. & Ball, R. C. Contact force distribution beneath a three-dimensional granular pile. *J. Phys. II* **7**, 1521–1532 (1997).
15. Vanel, L., Howell, D., Clark, D., Behringer, R. P. & Clément, E. Memories in sand: experimental tests of construction history on stress distributions under sandpiles. *Phys. Rev. E* **60**, R5040–R5043 (1999).
16. Serero, D., Reydellet, G., Claudin, P., Clément, E. & Levine, D. Stress response function of a granular layer: quantitative comparison between experiments and isotropic elasticity. *Eur. Phys. J. E* **6**, 169–179 (2001).
17. Goldenberg, C. & Goldhirsch, I. Force chains, microelasticity, and macroelasticity. *Phys. Rev. Lett.* **89**, 084302 (2002).
18. Reydellet, G. & Clément, E. Green’s function probe of a static granular piling. *Phys. Rev. Lett.* **86**, 3308–3311 (2001).
19. Cundall, P. A. & Strack, O. D. L. A discrete numerical model for granular assemblies. *Geotechnique* **29**, 47–65 (1979).
20. Otto, M., Bouchaud, J.-P., Claudin, P. & Socolar, J. E. S. Anisotropy in granular media: classical elasticity and directed-force chain network. *Phys. Rev. E* **67**, 031302 (2003).
21. Duffy, J. & Mindlin, R. D. Stress–strain relations and vibrations of a granular medium. *J. Appl. Mech.* **24**, 585–593 (1957).
22. Bathurst, R. J. & Rothenburg, L. Micromechanical aspects of isotropic granular assemblies with linear contact interactions. *J. Appl. Mech.* **55**, 17–23 (1988).
23. Chang, C. S. & Ma, L. Elastic material constants for isotropic granular solids with particle rotation. *Int. J. Solids Struct.* **29**, 1001–1018 (1992).
24. Gay, C. & da Silveira, R. Anisotropic elastic theory of preloaded granular media. *Europhys. Lett.* **68**, 51–57 (2004).
25. da Silveira, R., Vidalenc, G. & Gay, C. Stress propagation in two dimensional frictional granular matter. Preprint at (<http://arXiv.org/cond-mat/0208214>) (2002).
26. Johnson, K. L. *Contact Mechanics* 220 (Cambridge Univ. Press, Cambridge, 1985).
27. Tournat, V. Probing weak forces in granular media through nonlinear dynamic dilatancy: clapping contacts and polarization anisotropy. *Phys. Rev. Lett.* **92**, 085502 (2004).

**Acknowledgements** We thank A. P. F. Atman, R. P. Behringer, P. Claudin, E. Clément, J. Geng, N. Mueggenburg, M. van Hecke, W. van Saarloos and T. A. Witten for discussions. This work was supported by the Israel Science Foundation (ISF) and the US-Israel Binational Science Foundation (BSF).

**Competing interests statement** The authors declare that they have no competing financial interests.

**Correspondence** and requests for materials should be addressed to I.G. (isaac@eng.tau.ac.il).

## Nonlinear elasticity in biological gels

Cornelis Storm<sup>1\*</sup>, Jennifer J. Pastore<sup>2</sup>, F. C. MacKintosh<sup>3</sup>, T. C. Lubensky<sup>1,2</sup> & Paul A. Janmey<sup>1,2</sup>

<sup>1</sup>Department of Physics and Astronomy, University of Pennsylvania, 209 South 33rd Street, Philadelphia, Pennsylvania 19104, USA

<sup>2</sup>Institute for Medicine and Engineering, University of Pennsylvania, 3340 Smith Walk, Philadelphia, Pennsylvania 19104, USA

<sup>3</sup>Division of Physics and Astronomy, Vrije Universiteit Amsterdam, De Boelelaan 1081, 1081HV Amsterdam, The Netherlands

\* Present address: Instituut-Lorentz for Theoretical Physics, LION, Universiteit Leiden, PO Box 9506, NL-2300RA Leiden, The Netherlands

The mechanical properties of soft biological tissues are essential to their physiological function and cannot easily be duplicated by synthetic materials. Unlike simple polymer gels, many biological materials—including blood vessels<sup>1</sup>, mesentery tissue<sup>2</sup>, lung parenchyma<sup>3</sup>, cornea<sup>4</sup> and blood clots<sup>5</sup>—stiffen as they are strained, thereby preventing large deformations that could threaten tissue integrity. The molecular structures and design

principles responsible for this nonlinear elasticity are unknown. Here we report a molecular theory that accounts for strain-stiffening in a range of molecularly distinct gels formed from cytoskeletal and extracellular proteins and that reveals universal stress–strain relations at low to intermediate strains. The input to this theory is the force–extension curve for individual semiflexible filaments and the assumptions that biological networks composed of these filaments are homogeneous, isotropic, and that they strain uniformly. This theory shows that systems of filamentous proteins arranged in an open crosslinked mesh invariably stiffen at low strains without requiring a specific architecture or multiple elements with different intrinsic stiffness.

The filamentous architectures of two representative strain-stiffening networks—namely, neuronal intermediate filaments (the major cytoskeletal element of axons) and fibrin protofibrils (the fundamental polymers forming blood clots)—are shown in Fig. 1. These networks have large solvent-filled spaces, and their filaments are only gently curved between points of intersection. Stiffness, quantified by the shear moduli of a variety of biopolymer networks, is plotted as a function of applied strain in Fig. 2. Other studies have reported similar strain-stiffening in crosslinked actin<sup>6,7</sup>, keratin<sup>8</sup> and cytoplasmic gels<sup>6</sup>. The systems that we consider vary over orders of magnitude in stiffness and in the strains they tolerate: neurofilament networks can be deformed over 400% before failing, whereas actin networks rupture at strains of 20%.

The response of a single elastic filament to an applied force has been the subject of much study<sup>9–15</sup>. This force-response is dominated by entropy: because there are many curled-up configurations and only one that is perfectly straight, stretching a flexible filament reduces its conformational entropy and thus produces an opposing force. The ensuing elastic behaviour of semiflexible polymers is inherently nonlinear, as even modest strains pull the constituent filaments nearly straight, in marked contrast with conventional rubbers<sup>16</sup>.

Polymer theory distinguishes three types of filaments, characterized by two length scales: the persistence length  $l_p$  (the typical length scale for the decay of tangent–tangent correlations) and the contour length  $L_c$ . A filament is considered flexible when  $l_p \ll L_c$  and rigid when the opposite holds. Completely flexible filaments exhibit a purely entropic elastic response, whereas rigid filaments display no entropic elasticity. Most biologically relevant filaments are in a third intermediate category: semiflexible filaments with  $l_p$  and  $L_c$  of comparable magnitude. These filaments do not form loops and knots, yet they are sufficiently flexible to have significant thermal bending fluctuations. In networks, the relevant contour length is the distance between network junction points or crosslinks, which we also call  $L_c$  below.

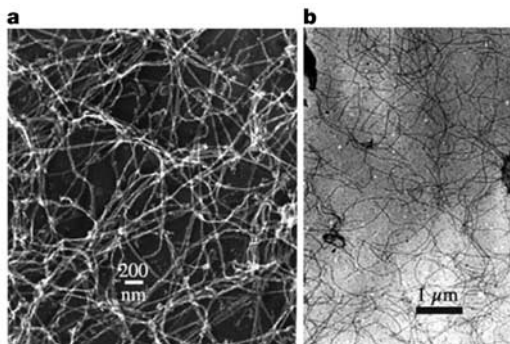


**Figure 1** Neurofilament and fibrin protofibril networks. These TEM images show the finite excess of filament contour length between crosslinks and overlap points. **a**, Metal-shadowed neurofilaments, and **b**, uranyl acetate-stained fibrin protofibrils, prepared as described in refs 25 and 26, respectively.

A theory for the force-response of such semiflexible filaments and the corresponding network shear modulus has been proposed<sup>12</sup>. This model is based on an energy functional of the form

$$E = \int_0^{L_c} dz \left\{ \frac{\kappa}{2} |\mathbf{u}''|^2 + \frac{f}{2} |\mathbf{u}'|^2 \right\} \quad (1)$$

where  $z$  is the projected coordinate along the end-to-end vector,  $\kappa$  is the bending stiffness (related to the persistence length as  $\kappa = k_B T l_p$ ) and  $f$  is the applied force.  $\mathbf{u}(z)$  describes the deviation of the filament from its straight conformation. The length  $L = L(f; L_c)$  of the end-to-end vector is calculated to harmonic order in  $\mathbf{u}(z)$  using the equipartition theorem<sup>17</sup> and the geometric relation between contour length and  $\mathbf{u}(z)$ . The result is most conveniently expressed in terms of the scaled difference between the extension at force  $f$  and that at zero force

$$\delta \tilde{L} = \frac{L(f; L_c) - L(0; L_c)}{L_c^2 / l_p} = \frac{1}{\pi^2} \sum_{n=1}^{\infty} \frac{\varphi}{n^2(n^2 + \varphi)} \quad (2)$$

where  $\varphi = f L_c^2 / \kappa \pi^2$  is a dimensionless force (see the inset to Fig. 3). The scaling force  $\kappa \pi^2 / L_c^2$  is the threshold force for the Euler buckling instability in thin cylinders<sup>18,19</sup>. Equation (2) can be inverted to yield a force–extension relation that, like the worm-like chain model applied to DNA<sup>9–11</sup>, diverges as  $f \sim (L - L_c)^{-2}$  as  $L \rightarrow L_c$ .

To get from the force–extension curve of single filaments to the

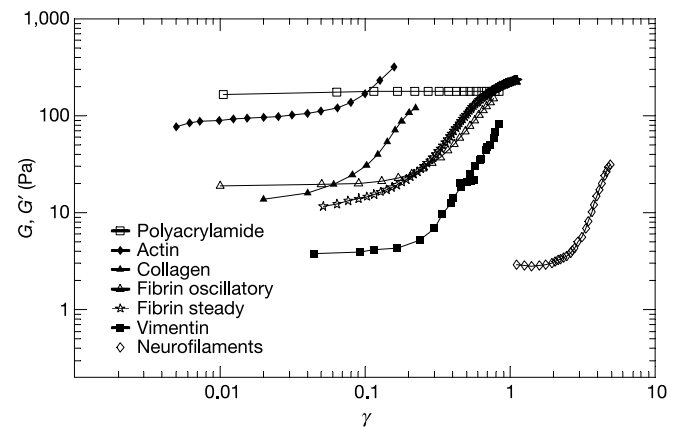


**Figure 2** Dynamic shear storage moduli measured at different strain amplitudes for a series of crosslinked biopolymer networks. The real part,  $G'$ , of the storage modulus reduces to the shear modulus  $G$  at zero frequency. Data shown are  $G'$  (at 10 rad  $s^{-1}$ ) values for F-actin, fibrin, collagen, vimentin and polyacrylamide, and shear modulus  $G$  for fibrin and neurofilaments, plotted as a function of the dimensionless strain  $\gamma$ . Dynamic shear moduli were measured in a strain-controlled rheometer (RFS-II, Rheometrics), which applies a sinusoidally varying strain with controllable maximal strain amplitude and computes the elastic storage moduli from the amplitude and phase shift of the resulting stress. Data analysis in the proprietary software assumes that the stress response is also a sinusoidal function, but in the nonlinear range of strains this relationship is not strictly true and the resulting stress function deviates from a sinusoid by having a sharper peak at maximal stress. To determine if this complication perturbs the reported strain-stiffening results, we also computed  $G$  by measuring stress at constantly increasing strains by using the steady rate function of the RFS-II, which imposes a constant increase in strain ( $5\% s^{-1}$ ) and reports the resulting stress at very small strain increments ( $<0.1\%$ ). The steady strain data overlap those from an oscillatory measurement of  $G'$  for the same sample of fibrin, verifying that oscillatory measurements accurately report the magnitude of strain stiffening under the conditions of our experiments. Sample preparation: F-actin/filamin gels were prepared as described<sup>27</sup>; vimentin ( $2 \text{ mg ml}^{-1}$ ) was a gift of P. Traub and prepared as described<sup>28</sup>; neurofilaments ( $3 \text{ mg ml}^{-1}$ ) were prepared as described<sup>23</sup>; rat tail collagen ( $2 \text{ mg ml}^{-1}$ ) was obtained from Sigma; polyacrylamide/bisacrylamide (5%) was polymerized with ammonium persulphate and TEMED by standard methods; fibrinogen was purified from salmon blood plasma as described<sup>29</sup> and dialysed into 50 mM Tris, 450 mM NaCl, pH 8.5, under which conditions only fibrin protofibrils form and lateral association into thicker bundles is prevented.

bulk elastic properties of filament networks requires a model for the network geometry. We consider a model isotropic network in which pairs of crosslink points (nodes) are connected by links composed of independent semi-flexible filaments. We assume that no torques are exerted at nodes so that filaments stretch or compress but do not bend in response to forces. We also assume that the network is sufficiently random that the filaments are isotropically distributed in the absence of stress. We allow for a distribution of end-to-end separations between nodes, with an average equal to  $L(f=0;L_c)$ , where  $L(f=0;L_c) = L_c(1 - L_c/6l_p)$  is the equilibrium end-to-end length of a polymer segment with a total contour length  $L_c$ . In response to external stresses, network nodes will displace and filaments will stretch or compress, that is, the network will strain. Under strain, the position  $\mathbf{R}_{0\alpha}$  of node  $\alpha$  in the unstrained network will transform to a new position  $\mathbf{R}_\alpha = \Lambda\alpha\mathbf{R}_{0\alpha}$  where  $\Lambda\alpha$  is the local (not necessarily symmetric) Cauchy deformation tensor. In random networks such as those we consider,  $\Lambda\alpha$  will in general depend on  $\alpha$ , that is, deformations will be non-affine. We make the simplifying assumption that deformations are affine, and take  $\Lambda\alpha = \Lambda$  independent of  $\alpha$ . Although there is no a priori reason to believe the affine approximation is valid, recent theoretical and experimental studies suggest that it is a good approximation for densely cross-linked filaments of high molecular weight<sup>20–22</sup>. As all forces are transmitted by links, and the force on each link is determined by its length, we can calculate the nonlinear stress tensor by averaging the force per area exerted by a single link over all magnitudes and directions of  $\mathbf{r}$ . The result is

$$\sigma_{ij}^T = \frac{\rho}{\det\Lambda} \left\langle f(|\Lambda\mathbf{r}|) \frac{(A_{ij}r_i)(A_{jk}r_k)}{|\Lambda\mathbf{r}|} \right\rangle_{P(\mathbf{r})}$$

where  $\rho$  is the number of links per unit volume and the average is over the probability distribution  $P(\mathbf{r})$  for separations  $\mathbf{r}$ . This stress tensor measures the force per unit area of the deformed sample and is symmetric.

We consider only the volume-conserving simple shear deformation produced in standard rheometers characterized by:

$$\Lambda = \begin{pmatrix} 1 & 0 & \gamma \\ 0 & 1 & 0 \\ 0 & 0 & 1 \end{pmatrix}$$

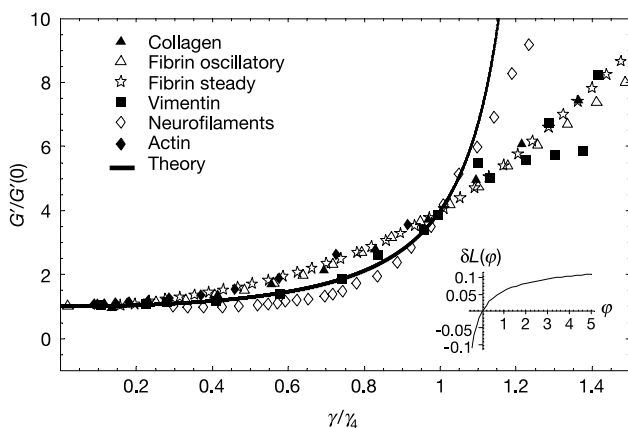


**Figure 3** Scaled modulus–strain curves for various biopolymer networks compared to theory and the scaled force–extension relation for a semiflexible polymer. Main panel, data of Fig. 2 scaled as described in the text (symbols) and theory (solid line). The theoretical curve was obtained assuming a uniform distribution of filament end-to-end lengths (that is, all equal to the mesh size), and averaging over all orientations in three dimensions. Inset, the dimensionless force versus extension curve described by equation (2).

In this case, the shear modulus is related to the  $xz$ -component of the stress tensor via  $G(\gamma) = \sigma_{xz}(\gamma)/\gamma$ .

To evaluate the shear modulus, we specify the bond probability distribution and force law  $f(L)$ . The simplest model is one in which  $f(L)$  is determined by equation (2) and the distribution function sets the distance between all nodes equal to the relaxed end-to-end length  $L(f=0;L_c)$  of the links, all of which we assume have the same contour length  $L_c$ . In this model, no new lengths are introduced by the averaging process, and the curve of shear modulus versus strain exhibits a universal scaling similar to that of the force–extension curve onto which data described by it will collapse. Figure 3 plots experimentally measured shear moduli  $G$  scaled by their value  $G_0$  at zero strain versus strain  $\gamma$  normalized by the strain  $\gamma_4$  at which  $G = 4G(0)$ . The value of 4 is arbitrarily chosen as the degree of stiffening that most systems examined exhibit before failure. The data collapse approximately onto the universal curve at modest strains, suggesting that the initial strain-stiffening in biopolymer networks is dominated by entropic effects that are well captured by our theory.

The theory developed thus far concerns only the low strain regime where entropic elasticity dominates. Figure 3 shows that at high strains departures from the theory become apparent, presumably because entropy alone does not capture all the physics of these systems.

We now modify the model to address these deviations, assuming that they arise from enthalpic contributions to  $f(L)$ , which we describe by introducing a stretch modulus  $K$ , measuring the longitudinal compliance of our previously inextensible filaments ( $K = \infty$ ). The force–extension relation, equation (2), for finite  $K$  becomes

$$L_K(f;L_c) = \left(1 + \frac{f}{K}\right)L\left(f\left(1 + \frac{f}{K}\right);L_c\right)$$

where  $L(f;L_c)$  is defined by equation (2). The persistence length and the stretch modulus of a rod are not independent: for a cylindrical tube of radius  $r$  they are related through<sup>23</sup>  $l_p/K = r^2/4k_B T$ .

The restriction that all filaments have the same end-to-end length is also not realistic, even if they have the same contour length. Crosslinking of thermally undulating filaments creates local pairwise node separations that differ from the zero-force end-to-end lengths of the filaments. By generalizing the classical theory of elasticity of crosslinked flexible polymers, we take the distribution function of end-to-end lengths of filaments in our network to be the equilibrium distribution of end-to-end lengths of semiflexible inextensible filaments of contour length  $L_c$  (ref. 24):

$$P(r) = \frac{2l_p}{L_c^2} \sum_{n=1}^{\infty} (\pi n)^2 (-1)^{n+1} \exp\left[-\frac{l_p(\pi n)^2}{L_c} \left(1 - \frac{r}{L_c}\right)\right]$$

An important consequence of having distributed lengths in this manner is that the network's filaments no longer individually experience zero force (as they do for a distribution with all lengths equal to the mean): some are stretched while others are compressed relative to their relaxed length. As a consequence, bulk mechanical equilibrium at zero isotropic stress will occur not at zero strain but at an isotropic strain described by a deformation tensor  $\Lambda_{0,ij} = \Lambda_0\delta_{ij}$ . The deformation  $\Lambda_0$  is determined by the condition that the isotropic part of the stress tensor  $\sigma^I\delta_{ij}$  vanishes. The angular average in the expression for the stress tensor in the presence of isotropic deformations is calculated to yield

$$\sigma^I(\Lambda_0) = \frac{\rho}{3\Lambda_0^2} \int_0^{L_c} dr r P(r)f(\Lambda_0 L(f=0;L_c)) = 0$$

as the condition determining  $\Lambda_0$ . This equation is solved numerically for particular parameter values.  $\Lambda_0$  is not an extra parameter—it is determined by the force–extension relation and the distribution function, both of which are functions of the persistence length, the

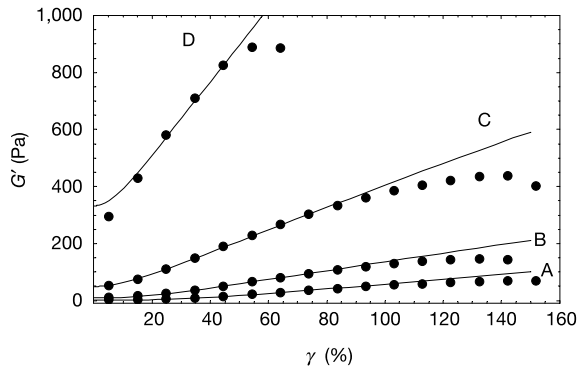


**Figure 4** Experimental data for fibrin protofilaments (dots) at various concentrations, and corresponding theoretical curves (solid lines) as computed from the extended theory including a stretch modulus. Best-fit values were determined for A–D as follows: A,  $c = 0.5 \text{ mg ml}^{-1}$  ( $\xi = 0.39 \text{ }\mu\text{m}$ ),  $K = 67 \text{ pN}$ ,  $\Lambda_0 = 0.948$ ; B,  $c = 1.0 \text{ mg ml}^{-1}$  ( $\xi = 0.27 \text{ }\mu\text{m}$ ),  $K = 58 \text{ pN}$ ,  $\Lambda_0 = 0.969$ ; C,  $c = 2.0 \text{ mg ml}^{-1}$  ( $\xi = 0.19 \text{ }\mu\text{m}$ ),  $K = 73 \text{ pN}$ ,  $\Lambda_0 = 0.981$ ; D,  $c = 4.5 \text{ mg ml}^{-1}$  ( $\xi = 0.12 \text{ }\mu\text{m}$ ),  $K = 110 \text{ pN}$ ,  $\Lambda_0 = 0.991$ . See text for definitions of parameters.

contour length and the stretch modulus only.

The extended theory makes specific predictions about how strain-stiffening scales with network density, and we test this by fitting to a series of modulus-strain curves for fibrin at different mass concentrations. Figure 4 shows the experimental data and the theoretical curves. The persistence length was experimentally determined to be  $0.5 \text{ }\mu\text{m}$  by computing the length scale for the decay of tangent–tangent correlations based on digitized microscopic images of fibrin filaments such as those in Fig. 1. The mesh size  $\xi$  of an isotropic network of polymers is calculated from the mass per unit length of polymer,  $\lambda$ , and the mass density,  $c$ . The number of links per unit volume is  $\rho = \lambda/cL_c = 3/(\xi^2L_c)$ . We assume that  $\xi \approx L_c$  so that  $\rho = 3/\xi^3$ . As  $\rho$ ,  $\xi$  and  $\Lambda_0$  are all determined by the mass concentration, our model has only one free parameter, the stretch modulus  $K$ . The best-fit values for  $K$  from Fig. 4 are of the order of 50–100 pN, very close to the elastic-rod estimate of  $K = 4k_B T l_p/r^2$  for a rod of radius  $r = 10 \text{ nm}$  and  $l_p = 0.5 \text{ }\mu\text{m}$ .

For all parameter values considered,  $\Lambda_0$  is smaller than, but of the order of, one, implying a small isotropic compression due to the asymmetric character of the single filament force–extension relation (see the inset to Fig. 3). As force rises steeply for extensions but remains relatively flat for compressions, stretched filaments contribute more to the residual stress after crosslinking, and the network as a whole will shrink.

Nonlinear elasticity, and specifically strain-stiffening, is generic to any network composed of semiflexible filamentous proteins. The degree of strain-stiffening can exceed tenfold increases in shear moduli under strains as small as 20%. The strain at which stiffening becomes significant depends strongly on the persistence length of the filament. Stiffer filaments, like F-actin or collagen, stiffen at a few per cent strain whereas more flexible filaments like vimentin stiffen only at larger strains, approaching 100%. The functional form of strain-stiffening at intermediate strain is generic for all semiflexible systems, but the maximal degree of strain-stiffening depends on such molecular details as the compliance of filaments to extension. Likewise, the strain at which the networks rupture also depends on the nature of the chemical bonds holding the filaments together.

These results have implications for cytoskeletal and other biopolymer networks. They suggest that the design of artificial biomaterials to replace tissues such as the arterial wall, whose function requires nonlinear elastic response<sup>1</sup>, could be facilitated by using polymers of stiffness and mesh size appropriate to produce strain-stiffening at the required range of deformations. Using this nonlinear passive elasticity, biological systems like the cytoskeleton

can actively manipulate their stiffness by local contraction of the network using motor proteins.

The inherent strain-stiffening of semiflexible polymer networks is only a starting point for the designs that have evolved to endow biological materials with their mechanical properties. Many strain-stiffening tissues have strikingly ordered stiff filaments co-assembled with an amorphous matrix. Variation of ordered elements in harder material like bone or wood provides other mechanisms to create nonlinear elasticity. The significance of the present work is that it shows such geometrical ordering is not required to produce the high degree of strain-stiffening that is an essential aspect of the elasticity of isotropic networks of crosslinked semiflexible polymers. □

Received 27 May 2004; accepted 7 March 2005; doi:10.1038/nature03521.

- Shadwick, R. E. Mechanical design in arteries. *J. Exp. Biol.* **202**, 3305–3313 (1999).
- Fung, Y. A *First Course in Continuum Mechanics* (Prentice Hall, Englewood Cliffs, 1994).
- Karakaplan, A. D., Bieniek, M. P. & Skalak, R. A mathematical model of lung parenchyma. *J. Biomech. Eng.* **102**, 124–136 (1980).
- Hjortdal, J. O. Extensibility of the normo-hydrated human cornea. *Acta Ophthalmol. Scand.* **73**, 12–17 (1995).
- Shah, J. V. & Janmey, P. A. Strain hardening of fibrin gels and plasma clots. *Rheologica Acta* **36**, 262–268 (1997).
- Janmey, P. A. et al. The mechanical properties of actin gels. Elastic modulus and filament motions. *J. Biol. Chem.* **269**, 32503–32513 (1994).
- Xu, J., Tseng, Y. & Wirtz, D. Strain hardening of actin filament networks. Regulation by the dynamic cross-linking protein alpha-actinin. *J. Biol. Chem.* **275**, 35886–35892 (2000).
- Ma, L., Xu, J., Coulombe, P. A. & Wirtz, D. Keratin filament suspensions show unique micromechanical properties. *J. Biol. Chem.* **274**, 19145–19151 (1999).
- Fixman, M. & Kovac, J. Polymer conformational statistics. III. Modified Gaussian models of stiff chains. *J. Chem. Phys.* **58**, 1564–1568 (1973).
- Smith, S. B., Finzi, L. & Bustamante, C. Direct mechanical measurement of the elasticity of single DNA molecules by using magnetic beads. *Science* **258**, 1122–1126 (1992).
- Marko, J. & Siggia, E. Stretching DNA. *Macromolecules* **28**, 8759–8770 (1995).
- MacKintosh, F., Käs, J. & Janmey, P. Elasticity of semiflexible biopolymer networks. *Phys. Rev. Lett.* **75**, 4425–4428 (1995).
- Kroy, K. & Frey, E. Force-extension relation and plateau modulus for wormlike chains. *Phys. Rev. Lett.* **77**, 306–309 (1996).
- Morse, D. Viscoelasticity of tightly entangled solutions of semiflexible polymers. *Phys. Rev. E* **58**, R1237–R1240 (1998).
- Gittes, F. & MacKintosh, F. C. Dynamic shear modulus of a semiflexible polymer network. *Phys. Rev. E* **58**, R1241–R1244 (1998).
- Treloar, L. R. G. *The Physics of Rubber Elasticity* (Clarendon, Oxford, 1975).
- Landau, L. D. & Lifshitz, E. M. *Statistical Physics I* (Pergamon, Oxford, 1980).
- Landau, L. D. & Lifshitz, E. M. *Theory of Elasticity* (Pergamon, Oxford, 1986).
- Gittes, F., Mickey, B., Nettleton, J. & Howard, J. Flexural rigidity of microtubules and actin filaments measured from thermal fluctuations in shape. *J. Cell Biol.* **120**, 923–934 (1993).
- Head, D. A., Levine, A. J. & MacKintosh, F. C. Deformation of cross-linked semiflexible polymer networks. *Phys. Rev. Lett.* **91**, 108102 (2003).
- Wilhelm, J. & Frey, E. Elasticity of stiff polymer networks. *Phys. Rev. Lett.* **91**, 108103 (2003).
- Gardel, M. L. et al. Elastic behavior of cross-linked and bundled actin networks. *Science* **304**, 1301–1305 (2004).
- Grosberg, A. Y. & Khokhlov, A. R. *Statistical Physics of Macromolecules* (American Institute of Physics Press, New York, 1994).
- Wilhelm, J. & Frey, E. Radial distribution function of semiflexible polymers. *Phys. Rev. Lett.* **77**, 2581–2584 (1996).
- Leterrier, J. F., Kas, J., Hartwig, J., Vegners, R. & Janmey, P. A. Mechanical effects of neurofilament cross-bridges. Modulation by phosphorylation, lipids, and interactions with F-actin. *J. Biol. Chem.* **271**, 15687–15694 (1996).
- Janmey, P. A. & Ferry, J. D. Gel formation by fibrin oligomers without addition of monomers. *Biopolymers* **25**, 1337–1344 (1986).
- Janmey, P. A., Hvidt, S., Lamb, J. & Stossel, T. P. Resemblance of actin-binding protein/actin gels to covalently crosslinked networks. *Nature* **345**, 89–92 (1990).
- Janmey, P. A., Euteneuer, U., Traub, P. & Schliwa, M. Viscoelastic properties of vimentin compared with other filamentous biopolymer networks. *J. Cell Biol.* **113**, 155–160 (1991).
- Wang, L. Z. et al. Purification of salmon clotting factors and their use as tissue sealants. *Thromb. Res.* **100**, 537–548 (2000).

**Acknowledgements** We are grateful to J.-F. Leterrier, S. Hvidt, P. Traub, J. Hartwig and E. Sawyer for collaboration in producing the protein networks and electron micrographs. This work was supported in part by the US-NIH and NSF/MRSEC programmes (P.A.J., T.C.L., C.S., J.J.P.) and by the Kavli Institute for Theoretical Physics at the University of California (E.C.M., P.A.J.), where some of this work was initiated.

**Competing interests statement** The authors declare that they have no competing financial interests.

**Correspondence** and requests for materials should be addressed to C.S. (cstorm@lorentz.leidenuniv.nl).